J. Fluid Mech. (2004), *vol.* 500, *pp.* 239–262.
DOI: 10.1017/S0022112003007353 Printed in the United Kingdom

Viscous instabilities in trailing vortices at large swirl numbers

By DAVID FABRE† AND LAURENT JACQUIN

ONERA, Fundamental and Experimental Aerodynamics Department, 9 rue des Vertugadins, 92190, Meudon, France

(Received 15 July 2002 and in revised form 2 July 2003)

This paper deals with the temporal stability of the q-vortex trailing line vortex model. We describe a family of viscous instabilities existing in a range of parameters which is usually assumed to be stable, namely large swirl parameters ($q > 1.5$) and large Reynolds numbers. These instabilities affect negative azimuthal wavenumbers ($m < 0$) and take the form of centre-modes (i.e. with a structure concentrated along the vortex centreline). They are related to a family of viscous modes described by Stewartson, Ng & Brown (1988) in swirling Poiseuille flow, and are the temporal counterparts of weakly amplified spatial modes recently computed by Olendraru & Sellier (2002). These instabilities are studied numerically using an original and highly accurate Chebyshev collocation method, which allows a mapping of the unstable regions up to $Re \approx 10^6$ and $q \approx 7$. Our results indicate that in the limit of very large Reynolds numbers, trailing vortices are affected by this kind of instability whatever the value of the swirl number.

1. Introduction

1.1. *Motivation*

Slender vortices are observed in a variety of aeronautical, environmental and astrophysical flows, and have been a focus of attention since the very first research in fluid mechanics. A number of recent studies on the topic have been motivated by the application to aircraft trailing wakes. In this case it is particularly crucial to predict the far-field behaviour of vortices in order to evaluate their potential impact on a following aircraft (see the review by Spalart 1998). A considerable amount of work has been devoted to the stability properties of vortex wakes, in order to identify the mechanisms of their decay and eventually to accelerate their dissipation.

A first class of instabilities, referred to as cooperative instabilities, occur in systems of two vortices or more, and are caused by the straining field induced on each vortex by the others. These instabilities were first investigated in the case of a pair of counter-rotating vortices with a simple core structure (Crow 1970; Moore & Saffman 1975; Tsai & Widnall 1976). In an effort to get closer to realistic aircraft trailing wakes, these studies were recently extended to more complex configurations, such as co-rotating vortex pairs (Le Dizès & Laporte 2002), multiple vortex configurations (Crouch 1997; Fabre, Jacquin & Loof 2002), as well as realistic vortex cores (Fabre & Jacquin 2003) and spatially evolving wakes (Fabre, Cossu & Jacquin 2000).

† Present address: Institut de Mécanique des Fluides, allée du professeur Soula, 31400, Toulouse, France; david.fabre@imft.fr

A second class of instabilities which concerns isolated vortices is due to the presence of a core axial flow. The description and mapping of these instabilities has also received considerable attention, using both numerical and asymptotic methods: see the papers by Lessen, Leibovich, Stewartson, Duck, Khorrami and coauthors in the list of reference. Most of these studies have taken as a base flow the generic model known as the q-vortex. This paper considers the temporal stability properties of this generic vortex model. The spatio-temporal properties of this flow have been considered recently (Delbende, Chomaz & Huerre 1998; Olendraru *et al.* 1999; Olendraru & Sellier 2002), and will not be addressed here. In the framework of temporal theory, the q-vortex is parameterized by two dimensionless parameters: the 'swirl number' q, which measures the relative amplitude of the swirl velocity compared to the axial velocity, and the Reynolds number Re. Therefore, the analysis consists of finding the complex frequencies $\omega(m, k; q, Re)$ of the eigenmodes as functions of their azimuthal and axial wavenumbers (m, k), and of the base flow parameters (q, Re).

1.2. *Review of previous work*

An overview of the temporal stability properties of the q-vortex may be found in Mayer & Powell (1992, referred to as MP in the following), or in the review by Ash & Khorrami (1995). In the strictly inviscid case ($Re = \infty$), the flow is unstable to perturbations with negative azimuthal wavenumbers ($m < 0$) within a limited range of swirl numbers. Helical modes ($m = -1$) possess the widest unstable range of swirl numbers. They are the only existing unstable modes in the limit $q = 0$, which corresponds to a non-rotating Gaussian jet, and they are stabilized above a critical swirl number $q_{crit} \approx 1.5$, a value first reported by Lessen *et al.* (1974). Larger values of $|m|$ (from $m = -2$ to -6) have also been considered numerically in detail (Lessen *et al.* 1974; Duck & Foster 1980; MP). These modes reach higher amplification rates, but they affect a more limited range of swirl numbers. In all these cases a critical swirl number slightly smaller than 1.5 was reported. For $|m| \gg 1$ instabilities become 'ring modes', i.e. modes with a structure localized in an annular region, and their properties are well described by the asymptotic study of Leibovich & Stewartson (1983). This study also predicts a lower bound for the critical swirl number: $q_{crit} \geqslant \sqrt{2}$. Stewartson & Capell (1985) refined this asymptotic theory to describe the vicinity of the critical swirl number. In this range, unstable modes become 'centre-modes', i.e. they become asymptotically concentrated in the vicinity of the vortex centreline. This behaviour results in numerical difficulties when computing marginally stable modes. This may explain why numerical studies failed to give a better approximation than $q_{crit} \approx 1.5$.

A number of studies were also conducted on the viscous problem, focusing on moderate values of the swirl number ($q < 1.5$). The asymptotic study of Stewartson (1982) demonstrated that viscosity has a purely stabilizing effect on the inviscid modes with $m < 0$. This result was verified numerically by MP. Moreover, two kinds of purely viscous modes have been found by Khorrami (1991) and Duck & Khorrami (1992), corresponding to azimuthal wavenumbers $m = 0$ and $m = +1$. These modes occur for $q < 1.3$, and their growth rates are always several orders of magnitude smaller than those of the corresponding inviscid modes.

Up to now, the range of parameters corresponding to large swirl numbers ($q > 1.5$) and large Reynolds numbers ($Re \geqslant 10^3$) does not seem to have been studied in the framework of temporal stability theory. However, there are several indications of the existence of unstable modes in this range. First, the asymptotic study of Stewartson & Brown (1985) leads to the prediction of weakly unstable modes in the vicinity of the curve $k = -m/q$ in some intervals of swirl numbers. The largest instability interval

is found for helical modes ($m=-1$) and corresponds to $1.77 \leqslant q \leqslant 2.31$. These modes are characterized by a complex structure: they display both a centre-mode behaviour, and a critical layer singularity. Due to the critical layer, these modes can only be justified as an eventual limit of modes computed using the viscous equations with vanishing viscosity. These rather bizarre results (according to the authors' own words) seem to have been overlooked by most authors. The only relevant study is that of Duck (1996), who concluded that viscosity has a purely stabilizing effect on these modes. However, he applied his results to a different range than considered here, namely to values of q close to 0.4 and 0.8.

A second indication of the existence of instabilities for large swirl numbers may be found in the work of Stewartson *et al.* (1988), referred to as SNB in the following, who considered the related problem of swirling Poiseuille flow (i.e. a rotating flow in a duct). They demonstrated the existence of a family of viscous unstable centre-modes occurring for large values of the Reynolds number. In their conclusions, SNB suggested that a similar family of viscous modes may exist in the q-vortex, and may affect all values of the swirl number q in the limit $Re \to \infty$. This point does not seem to have been explored further. A final indication of the existence of instabilities for large swirl numbers comes for the work of Olendraru & Sellier (2002), who considered the spatio-temporal stability properties of the q-vortex. They observed for $Re=10^4$ the existence of spatially unstable modes up to $q \approx 3$ for both $m=-1$ and $m=-2$. Olendraru & Sellier (2002) suggested that these modes could be the spatial counterparts of the modes predicted by Stewartson & Brown (1985). However, the modes observed by Olendraru & Sellier (2002) occur in a continuous range of swirl numbers, and not in discrete intervals as predicted by Stewartson & Brown (1985). Since their objective was mainly the mapping of the region of absolute instability, Olendraru & Sellier (2002) did not explore this problem further.

1.3. *Goal of the present work*

The first goal of the present work is to complete the topography of instabilities of the q-vortex, as presented by MP, by a mapping of the region corresponding to high swirl numbers ($q > 1.5$) and moderately high Reynolds numbers (up to $Re \approx 10^6$). We show that while viscosity is purely stabilizing for small Reynolds numbers, it becomes destabilizing for $Re \gtrsim 10^3$. As the Reynolds number is increased above this order of magnitude, instabilities with negative azimuthal wavenumbers ($m<0$) exist for swirl numbers well above the inviscid threshold. For example, for $Re=10^4$, the critical swirl numbers associated with helical ($m=-1$) and double-helix ($m=-2$) modes correspond respectively to $q_{crit}=3.235$ and 2.763, about double the inviscid threshold $q_{crit} \approx 1.5$. Moreover, our numerical results indicate that instabilities may be present for all values of q in the limit of vanishing (but non-zero) viscosity.

The second goal is to clarify the nature of these instabilities. We show that they are distinct from the inviscid-type instabilities occurring for $q<1.5$, as well as from the viscous modes of Khorrami (1991) and from the near-neutral inviscid centre-modes considered by Stewartson & Brown (1985). On the other hand, they are related to the viscous centre-modes discovered by SNB in the swirling Poiseuille flow.

The paper is organized as follows. Section 2 is devoted to the description and validation of the numerical method, an original and highly accurate Chebyshev collocation method. It is shown in particular that this method allows high-precision results with only half of the number of collocation points required by related methods. In § 3 the topography of instabilities is described up to $Re=10^4$ for $m=-1$ and -2. Then, the trends for larger values of $|m|$ and Re are briefly addressed. In § 4, some

characteristic features of these instabilities are detailed, in particular the behaviour of the secondary unstable branches and the structure of the eigenmodes. Then, the relation of these modes to other families of instabilities are discussed. In § 5, the relevance of the present results with respect to aircraft trailing wakes is discussed. Finally, § 6 summarizes the results.

2. Problem formulation and numerical treatment

2.1. *Base flow*

The base flow used here is the well-known q-vortex trailing line vortex model. Using cylindrical polar coordinates (r, θ, z), the radial, azimuthal and axial velocity components of this model are defined in non-dimensional form as follows:

$$U(r) = 0, \quad V(r) = q/r\left(1 - \mathrm{e}^{-r^2}\right), \quad W(r) = \mathrm{e}^{-r^2}. \tag{2.1}$$

This base flow is characterized by two dimensionless parameters: the swirl parameter q and the Reynolds number Re (which is based on the axial velocity scale and the dispersion radius of vorticity). Note that a uniform advection of amplitude a is sometimes added to the axial velocity in the model. This parameter is not relevant for the temporal stability problem because of Galilean invariance, and here it is set to zero as in Lessen & Paillet (1974).

The q-vortex corresponds to a simplification of the Batchelor (1964) vortex, namely a spatially evolving similarity solution of the incompressible Navier–Stokes equations under a quasi-parallel approximation. It has been successfully used to fit a variety of experiments, such as vane-guide-generated pipe flows, and trailing vortices with moderate Reynolds numbers. On the other hand, as emphasized by Spalart (1998), the Batchelor (1964) solution cannot be considered as a relevant model for trailing vortices originating from high-aspect-ratio wings at high Reynolds numbers. In such vortices the vorticity and axial velocity fields are far from Gaussian, and in order to describe them at least two core radius measures have to be introduced. This was particularly shown by Jacquin *et al.* (2001), who investigated experimentally the wake of an A300 model up to a downstream distance of 9 wing spans. In order to fit the azimuthal velocity field of the vortices, they introduced a 'two core scales model' which is composed of a very narrow 'internal core' in solid-body rotation embedded in an 'external core' where the velocity decreases following a power law. A similar structure was proposed for the axial velocity field. The 'inner' and 'outer' core radii characterizing this model were evaluated to be respectively 1% and 10% of the wing span.

The Batchelor (1964) solution has been criticized from a mathematical point of view, because of the non-uniquess of the solution and because of the inherent parallel approximation (Uberoi 1979). Its failure to describe realistic trailing vortices can also be explained with physical arguments, already raised by Moore & Saffman (1973). Basically, this solution describes the viscous diffusion of a flow originating from a line vortex at the inlet plane. Such an inlet condition would result from a 'rectangular' wing lift distribution, and this situation is unrealistic. Real-life trailing vortices are not formed in this way, but rather through the roll-up of a vortex sheet, and possibly through the merging of several vortex cores. These mechanisms are essentially inviscid, and viscous diffusion (laminar or turbulent) is not expected to play any role after completion of the roll-up.

In conclusion, the q-vortex is not fully representative of real vortices such as those found behind aircraft. But it remains sufficiently meaningful, mathematically

and physically, for studying the physics of three-dimensional slender vortices and in particular the linear dynamics resulting from the coupling between tangential shear and axial shear. In this respect, this model is sufficiently rich to justify its almost universal use in stability analyses.

2.2. *Viscous stability equations*

In the stability analysis we consider infinitesimal disturbances in the form of eigenmodes, characterized by an axial wavenumber k, an azimuthal wavenumber m, and a complex frequency ω, i.e.

$$(u'_r, u'_\theta, u'_z, p') = [u(r), v(r), w(r), p(r)] \exp(\mathrm{i}kz + \mathrm{i}m\theta - \mathrm{i}\omega t). \tag{2.2}$$

Linearization of the continuity, r-, θ- and z-momentum equations leads to the following set of equations:

$$\left(\partial_r + \frac{1}{r}\right) u + \frac{\mathrm{i}m}{r} v + \mathrm{i}kw = 0, \tag{2.3a}$$

$$\mathrm{i}(m\Omega + kW - \omega)u - 2\Omega v + \partial_r p = \frac{1}{Re}\left[\left(\partial_r^2 + \frac{1}{r}\partial_r - k^2 - \frac{m^2+1}{r^2}\right) u - \frac{2\mathrm{i}m}{r^2} v\right], \tag{2.3b}$$

$$\mathrm{i}(m\Omega + kW - \omega)v + \Xi u + \frac{\mathrm{i}m}{r} p = \frac{1}{Re}\left[\left(\partial_r^2 + \frac{1}{r}\partial_r - k^2 - \frac{m^2+1}{r^2}\right) v + \frac{2\mathrm{i}m}{r^2} u\right], \tag{2.3c}$$

$$\mathrm{i}(m\Omega + kW - \omega)w + W'u + \mathrm{i}kp = \frac{1}{Re}\left(\partial_r^2 + \frac{1}{r}\partial_r - k^2 - \frac{m^2}{r^2}\right) w. \tag{2.3d}$$

Here $\Omega(r) = V(r)/r$ denotes the rotation rate, and $\Xi(r) = V(r)/r + V'(r)$ is the mean flow axial vorticity. Differentiation with respect to r is denoted by primes for the mean flow quantities, and by ∂_r for perturbations.

To resolve this system, one can conveniently reduce the number of unknown functions from four to two by elimination of the axial velocity and pressure components. This leads to a system for $[u(r), v(r)]$ which can be put into the following symbolic form:

$$\omega \mathscr{L} \begin{pmatrix} -\mathrm{i}u \\ v \end{pmatrix} = \left(\mathscr{M} - \frac{\mathrm{i}}{Re}\mathscr{D}\right) \begin{pmatrix} -\mathrm{i}u \\ v \end{pmatrix}. \tag{2.4}$$

The components of the matrices $\mathscr{L}, \mathscr{M}, \mathscr{D}$ are differential operators with real coefficients, which are detailed in the Appendix. This reduced system can be considered as the cylindrical version of the coupled Orr–Sommerfeld and Squire equations. It takes the form of a generalized eigenvalue problem for the frequency ω. This is convenient for a temporal stability analysis, and makes the numerical resolution using a global matrix eigenvalue method straightforward. Note, however, that the reduced form (2.4) is not valid in the two-dimensional case ($k = 0$), because in this case the radial and azimuthal velocity components (u, v) cannot be considered as independent functions. Therefore our method cannot be expected to be accurate in the limit of very long wavelengths ($k \to 0$).

Let us consider now the limit conditions to be satisfied by the eigensolutions. At $r = \infty$, according to Lessen & Paillet (1974), the unknown functions must decrease exponentially for $k \neq 0$ (and algebraically for $k = 0$, a case that will not be considered here). At the axis of the vortex ($r = 0$), the use of cylindrical coordinates leads to a regular singularity in the equations. The physically relevant solutions, which must be continuous and single-valued, can be expanded as Taylor series at $r = 0$. The limit

conditions can be deduced from inspection of the leading-order terms of the Taylor series, and depend upon the azimuthal wavenumber m. For $m=0$:

$$u = O(r), \quad v = O(r), \quad w = O(1), \quad p = O(1); \tag{2.5a}$$

and for $|m| \neq 0$:

$$u = O(r^{|m|-1}), \quad v = O(r^{|m|-1}), \quad w = O(r^{|m|}), \quad p = O(r^{|m|}), \tag{2.5b}$$

and

$$\lim_{r=0} \frac{|m|u + \mathrm{i}mv}{r^{|m|-1}} = 0. \tag{2.5c}$$

Note, finally, that the functions u, v, w, p on the interval $[0, \infty]$ can be extended to functions on $[-\infty, \infty]$, and that the parity of these functions depends upon m: for m odd (respectively even), w, p are odd (respectively even) and u, v are even (respectively odd). The numerical resolution method takes advantage of this property.

2.3. *Description of the numerical method*

The numerical method used here is a Chebyshev spectral collocation method. This kind of method was first applied to the stability of swirling flows by Khorrami *et al.* (1989). Since then it has been used in most of the stability analyses (Khorrami 1991, 1992; MP; Olendraru & Sellier 2002). The method used here differs from other implementations by a few points, which are described below. A more complete description can be found in Fabre (2002).

First, the problem has to be mapped from physical space to Chebychev space ($\xi \in [-1, 1]$) via a mapping function $r = \phi(\xi)$. For this purpose, previous contributors have truncated the problem to a finite interval $r \in [0, R_{max}]$, and have proposed and discussed various mapping functions. Here, the eigenfunctions are considered as functions of $r \in [-\infty, \infty]$, and are mapped to Chebyshev space by the following algebraic mapping:

$$r = \phi(\xi) = \frac{H\xi}{1-\xi^2}. \tag{2.6}$$

This mapping function depends upon a single parameter H which controls the spreading of the collocation points: about half of the collocation points in physical space occupy $|r_j| < H$.

Then, instead of using all of the Chebyshev polynomials, the parity properties of the unknown functions are taken into account, and the following expansions are used:

$$F(\xi) = \sum_{j=0}^{N} a_j T_{2j}(\xi) \tag{2.7}$$

for even functions, and

$$F(\xi) = \sum_{j=0}^{N} a_j T_{2j+1}(\xi) \tag{2.8}$$

for odd functions. In both cases, the collocation points in Chebyshev space are chosen as the $N+1$ positive roots of the Chebyshev polynomial of order $2N+2$:

$$\xi_j = \cos\left(\frac{(2j+1)\pi}{4N+4}\right), \quad j = 0, N. \tag{2.9}$$

These points correspond to half of the Gauss points of a complete expansion of order $2N+1$. The collocation points in physical space are deduced through $r_j = \phi(\xi_j)$. The

parity properties of the unknown functions are introduced into the definition of the differential operators appearing in (2.4). Note that this leads to different schemes for odd and even values of m. The great advantage of this method is that with $N+1$ collocation points, we are actually handling a Chebyshev expansion of order $2N$ for an even function, and $2N+1$ for an odd function.

Finally, in the present method, no limit conditions are imposed on the unknown functions. As discussed by Canuto *et al.* (1988), the use of a Chebyshev expansion in conjunction with an algebraic mapping leads to an exponential convergence provided that the functions to be computed decay at least algebraically as $r \to \infty$, a property which is verified here. At $r = 0$, functions admitting an expansion of the form (2.7) or (2.8) do not necessarily satisfy the limit conditions (2.5), except for the case of axisymmetric modes ($m = 0$). However, as will be illustrated below, for converged modes the limit conditions are effectively satisfied with spectral accuracy.

It is known that a spectral method generally leads to a large number of spurious unconverged couples of eigenvalues/eigenvectors, and a rule is needed to identify the physically relevant modes. Two convergence criteria have been used for this purpose. The first one is the 'spectral residual', which is defined, for a function with a spectral expansion of the form (2.7) or (2.8), as the relative 'weight' of the 10% of coefficients of larger order in the expansion, i.e.

$$C_s = \left(\sum_{j=N-N/10}^{N} |a_j|^2 \right) \Big/ \left(\sum_{j=0}^{N} |a_j|^2 \right). \tag{2.10}$$

A value of C_s close to zero indicates that the eigenfunction does not contain any short-wave oscillations, as expected for converged modes. The second criterion is defined, for $m \neq 0$, as the value of the limit condition at the axis given by (2.5*c*):

$$C_0 = \lim_{r=0} \frac{|m|u + \mathrm{i}mv}{r^{|m|-1}}, \tag{2.11}$$

where u and v are replaced by their spectral approximations. Other convergence tests were performed. In particular, it was carefully checked that the retained modes also satisfied the limit conditions at $r \to \infty$. Moreover, in some cases the results were compared to those obtained with a second eigenvalue problem arising from the adjoint stability equations. These verifications showed that the criteria C_s and C_0 defined above are sufficient to discriminate accurately the converged modes from the spurious ones. Typically, an eigenmode can be considered as spectrally converged when both these criteria are smaller than 10^{-8}.

2.4. *Validation of the numerical method*

To illustrate the efficiency of the method, we present convergence histories for three test cases which are already documented in previous work. For each case we display the computed amplification rate ω_i as function of the number of collocation points N and the mapping parameter H. The first case, displayed in table 1, corresponds to the most unstable inviscid mode for $q = 0.5$, $m = -1$, $k = 0.5$. For this case, MP gave a converged value with 13 significant digits, using as many as 200 collocation points. The second case, displayed in table 2, corresponds to the viscous axisymmetric mode with $m = 0$, $q = 1$, $k = 0.5$, $Re = 10^4$ used by Khorrami (1991) as a convergence test. The third case, displayed in table 3, corresponds to $m = -1$, $q = 0.4$, $k = 2.01123$, $Re = 10^4$ where a crossing between two modes of instability has been documented by Khorrami (1992). The values of the convergence C_s and C_0 are also displayed in

N	H	ω_i	C_s	C_0
40	2	0.20262810	5×10^{-15}	5×10^{-10}
60	2	0.202628101	5×10^{-17}	3×10^{-11}
80	4	0.20262810129	1×10^{-21}	1×10^{-13}
100	4	0.2026281012941	3×10^{-26}	1×10^{-14}
130	6	0.2026281012941	2×10^{-23}	1×10^{-14}
MP 200	–	0.2026281012942	–	

TABLE 1. Convergence history of the Chebyshev method, as a function of the number of collocation points N and the mapping parameter H. Case I: most amplified mode for $q=0.5$, $m=-1$, $k=0.5$ (inviscid case). MP: Result from Mayer & Powell (1992).

N	H	ω_i	C_s
20	2	1.84×10^{-4}	1×10^{-7}
25	2	1.8469×10^{-4}	1×10^{-8}
32	2	1.8469080×10^{-4}	5×10^{-11}
50	2	1.84690800×10^{-4}	9×10^{-17}
50	4	1.84690800×10^{-4}	3×10^{-13}
80	2	$1.8469080002\times10^{-4}$	9×10^{-24}
80	4	$1.8469080002\times10^{-4}$	9×10^{-22}
K 50	–	1.8468×10^{-4}	–

TABLE 2. Convergence history of the Chebyshev method. Case II: most amplified mode for $q=1$, $m=0$, $k=0.5$, $Re=10^4$. K: result from Khorrami (1991).

N	H	Mode 1	Mode 2
40	1	8.15×10^{-3}	8.15×10^{-3}
50	1	8.1530×10^{-3}	8.1575×10^{-3}
60	1	8.153070×10^{-3}	8.157574×10^{-3}
80	1	8.1530702×10^{-3}	8.15757484×10^{-3}
100	1	8.1530702×10^{-3}	8.15757484×10^{-3}
K 100	–	8.1530×10^{-3}	8.1575×10^{-3}

TABLE 3. Convergence history of the Chebyshev method. Case III: modes 1 and 2 for $q=0.4$, $m=-1$, $k=2.01123$, $Re=10^4$. K: result from Khorrami (1992).

table 1 and C_s in table 2, and the effect of a variation of the mapping parameter H with fixed N is illustrated in table 2.

In all these cases, the same precision as previously reported has been obtained using a number of collocation points smaller by a factor 2. This factor 2 can be attributed to the use of the symmetry conditions in the Chebyshev expansion: with $N+1$ collocation points, we are actually handling a Chebychev expansion of order $2N$. Considering that the computational time required to solve an eigenvalue problem scales as the cube of the dimension of the matrices, a factor 8 is actually gained. The gain is even better if we recall that we are using a reduced system in terms of the eigenfunctions u and v, instead of the starting equations for u, v, w, p.

Thus, the method is convenient for scanning rapidly and efficiently large regions of the space of parameters. Note, however, that the efficiencies of the present scheme are specific to the temporal stability analysis of axisymmetric flows. As such, the approach

	Overall maximum of amplification			Critical swirl number		Neutral mode with largest k	
	ω_i^{max}	q	k	q_{crit}	k	q	k
$m=-1$, $Re=10^2$	0.1734	0.406	0.769	1.146	0.490	0.269	1.714
$m=-1$, $Re=10^3$	0.2339	0.448	0.811	1.793	0.306	0.282	2.278
$m=-1$, $Re=10^4$	0.2416	0.457	0.812	3.235	0.160	0.189	3.375
$m=-1$, NV	0.2424	0.458	0.811	≈ 1.5	≈ 0.54	≈ 0.42	≈ 2
$m=-2$, $Re=10^2$	0.1812	0.622	1.108	1.173	0.736	0.616	1.957
$m=-2$, $Re=10^3$	0.2956	0.680	1.174	1.673	0.736	0.515	2.597
$m=-2$, $Re=10^4$	0.3119	0.691	1.180	2.763	0.375	0.236	4.711
$m=-2$, NV	0.3138	0.693	1.182	≈ 1.5	≈ 1.1	≈ 0.7	≈ 2.4
$m=-3$, $Re=10^2$	0.1431	0.656	1.582	1.108	1.769	0.880	2.434
$m=-3$, $Re=10^3$	0.3245	0.761	1.659	1.536	1.346	0.493	3.660
$m=-3$, $Re=10^4$	0.3514	0.776	1.664	2.280	0.784	0.265	6.664
$m=-3$, NV	0.3546	0.779	1.665	≈ 1.5	–	–	–

TABLE 4. Dependence on the Reynolds number of some properties of the instability region for $m=-1$, -2 and -3: overall maximum amplification rate ω_i^{max} and corresponding swirl number and wavenumber; critical swirl number q_{crit} and wavenumber of the corresponding neutral mode; swirl number and wavenumber of the neutral mode with the smallest wavelength. The results displayed for the inviscid case (NV) are those of MP.

cannot be tailored into a general eigenvalue solver (performing both temporal and spatial analyses) for an arbitrary mean flow.

In the remainder of this work, the mapping parameter was generally set to $H=1$, and in some cases to $H=0.5$ in order to concentrate a larger number of collocation points close to the vortex centreline, where the structure of the modes is more complex. The number of collocation points was increased with the Reynolds number, from $N=60$ for $Re=100$, up to $N=280$ for $Re=10^6$.

3. Topography of instabilities

In this section, we describe the topography of instabilities for helical ($m=-1$) and double-helix ($m=-2$) modes, for Reynolds numbers ranging from $Re=10^2$ to 10^4. Then we briefly describe the extent of the instability domain and the variation of the amplification rate for larger values of $|m|$ and Re.

3.1. *Helical modes* ($m=-1$)

Consider, first, the case of helical modes ($m=-1$). Figure 1 displays iso-levels of the amplification rate of the most amplified mode in the (q,k)-plane, the outermost contour being the neutral stability curve. In this plot the thick dashed line corresponds to the stability curve in the inviscid case, reproduced from figure 3 of MP. Note that we consider the regions of parameters $m<0$, $q>0$, whereas MP's figures correspond to $m>0$, $q<0$; due to the symmetries of the problem both choices are equivalent.

For $Re=10^2$ (figure 1*a*), the instability region is smaller than in the inviscid case, and the flow is completely stabilized above a critical swirl number of $q_{crit}=1.146$. This value is substantially smaller than the inviscid threshold $q_{crit}\approx 1.5$. Moreover, within the unstable region the amplification rates are always smaller than in the inviscid case. According to table 4, the overall maximum of amplification is about 30% weaker than

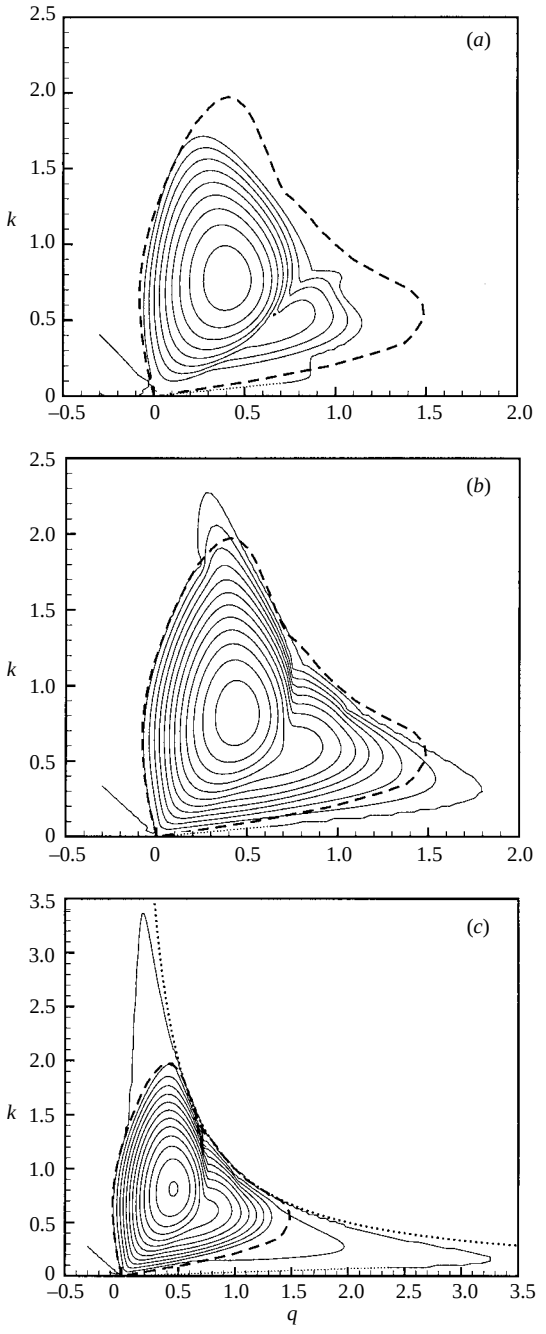

FIGURE 1. Topography of the most unstable mode in the (k, q)-plane, for $m = -1$ and (*a*) $Re = 10^2$, (*b*) 10^3, and (*c*) 10^4. Contours of constant amplification rate ω_i (outermost contour is the neutral curve, spacing between contours is 0.02). The thick dashed line corresponds to the neutral curve in the inviscid case (from MP). Plot (*c*) for $Re = 10^4$ also displays as a dotted line the curve of equation $k = -m/q$ which approximates the upper neutral curve. The dotted portions of the lower neutral curves are inferred (not computed).

in the inviscid case, and the corresponding position in the (q, k)-diagram is somewhat different. On the other hand, the unstable region located in the range $-0.074 < q < 0$ is only weakly affected by viscosity, and the neutral curve is close to the inviscid one. It can be remarked that the unstable region displays a two-lobed structure, with a prominent ridge separating the lobes. This characteristic feature was also observed in the inviscid case by MP. For $Re = 100$ the position of the ridge is slightly displaced towards smaller q and k.

For the range of parameters considered so far, it may be concluded that viscosity has a purely stabilizing effect on the instabilities. This behaviour is consistent with the asymptotic study of Stewartson (1982), and with the observations in § 3.2 of MP. We recall that MP considered even smaller values of the Reynolds numbers, and observed an elimination of the unstable region at $Re = 13.9$. As we shall see now, a different picture is obtained when considering larger values of the Reynolds number.

Figure 1(*b*) presents the case $Re = 10^3$. In this case, the unstable region has a larger extent than in the inviscid case. It extends both towards large q (for small k) and towards large k (for small q). The critical swirl number for stabilization is now $q_{crit} = 1.793$, and the unstable mode with the largest wavenumber corresponds to $k = 2.281$. On the other hand, in the range of parameters where inviscid instabilities exist, viscosity remains generally stabilizing, and the amplification rates are slightly smaller than the inviscid results of MP. For example, the overall maximum amplification rate is now $\omega_i = 0.2339$, nearly 3% smaller than in the inviscid case, and it is found at approximately the same position in the (q, k)-diagram (see table 4).

Figure 1(*c*) corresponds to $Re = 10^4$. The unstable region is now observed to extend well beyond the inviscid threshold. The critical swirl number is $q_{crit} = 3.235$, more than twice that in the inviscid case. This is in reasonable agreement with the value $q \approx 3.1$ obtained by Olendraru & Sellier (2002) using spatial stability analysis. Note that in the central parts of the instability region the amplification rates are very close to the inviscid results. For example, the overall maximum amplification rate corresponds to $\omega_i = 0.2416$, nearly 0.3% smaller than in the inviscid case, and it occurs for the same values of k and q. Figure 1(*c*) also displays as a dotted line the hyperbola of equation $k = -m/q$. In the range $0.5 < q < \sqrt{2}$, this curves closely corresponds to the upper neutral curve of both the $Re = 10^4$ and the inviscid results. In the inviscid case this property was predicted by the asymptotic analysis of Stewartson & Capell (1985). Moreover, in the ranges $q < 0.5$ and $q > \sqrt{2}$, the hyperbola still gives a good estimate of the upper neutral curve in the viscous case.

Note that a second instability region is also apparent in the lower left corners of plots 1(*a–c*), approximately in the range of parameters delimited by $q < 0$, $0 < k < |q|$. This region corresponds to the viscous instability identified by Khorrami (1991). The topography of this instability has already been described in detail by MP (see their figure 11). It extends down to about $q = -1.1$, outside the range of parameters considered in our study.

3.2. *Double-helix modes* ($m = -2$)

Figure 2 displays the topography of instabilities for double-helix modes ($m = -2$), with the same set of Reynolds numbers, and with the same representation conventions as in figure 1. Results display the same trends as for $m = -1$. For $Re = 10^2$ (figure 2*a*), viscosity is purely stabilizing and the instability region has a smaller extent than in the inviscid case. Here the critical swirl number is reached at $q_{crit} = 1.173$, and the overall maximum of amplification corresponds to $\omega_i^{max} = 0.1812$, a value 40% smaller than in the inviscid case (which corresponds to $\omega_i^{max} = 0.3138$). Recall that MP reported

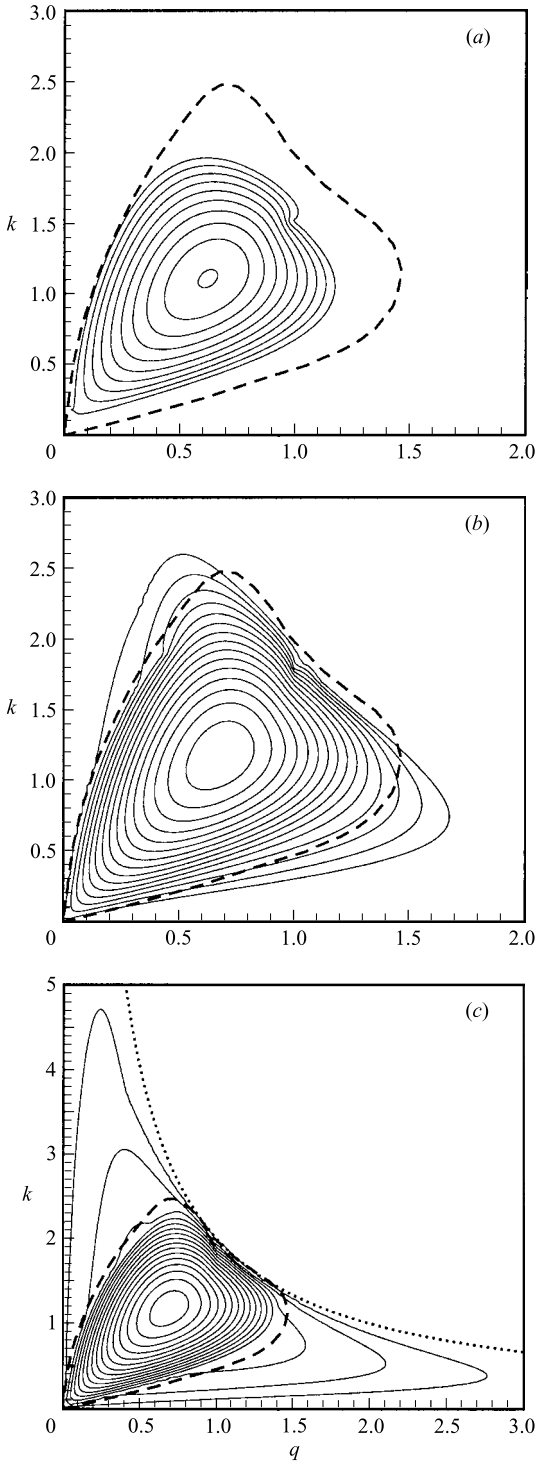

FIGURE 2. As figure 1, but for $m = -2$ and (*a*) $Re = 10^2$, (*b*) 10^3, and (*c*) 10^4.

a complete stabilization of the flow below a Reynolds number of $Re = 27.3$. For $Re = 10^3$ (figure 2*b*), the unstable region extends beyond the inviscid neutral curve. For this case the critical swirl number is $q_{crit} = 1.673$. On the other hand, viscosity remains stabilizing in the range of parameters where an inviscid stability occurs. For example, the maximum amplification rate, reported in table 4, is nearly 6% weaker than in the inviscid case. Finally, for $Re = 10^4$ (figure 2*c*), the critical swirl number is $q_{crit} = 2.763$. As for helical modes, this value is about twice that in the inviscid case. It is also in agreement with the value $q \approx 2.7$ obtained by Olendraru & Sellier (2002) using spatial stability analysis. As for $m = -1$, the curve of equation $k = -m/q$ closely corresponds to the upper neutral curve in the region of inviscid instability and gives an upper bound to this neutral curve in the regions of purely viscous instability.

3.3. *Trends for larger m and Re*

The results for $m = -3$ are qualitatively similar to the $m = -2$ case and are not displayed. For Reynolds numbers of $Re = 10^2$, 10^3 and 10^4, the critical swirl numbers correspond respectively to $q_{crit} = 1.108$, 1.536 and 2.280. Table 4 presents several quantitative results obtained for $m = -1$, -2 and -3. We display the value and the location of the overall maximum amplification rate ω_i^{max}, the critical swirl number q_{crit} and the corresponding wavenumber, and the location of the neutral mode with the largest wavenumber. The corresponding results in the inviscid case, reproduced from MP, are also displayed.

For values of Re, q and m larger than those considered above, the complete mapping of the unstable region becomes a difficult numerical task. The difficulties are partly due to the structure of the unstable modes, which become more and more singular as the Reynolds number is increased, as will be illustrated in § 4.2. Difficulties are also due to the fact that instability affects long wavelengths (small k), a region where our numerical method is less accurate. Note that this latter difficulty prevented us from determining exactly the lower marginal curve for $m = -1$ in figure 1(*a–c*). Despite these difficulties, figures 1 and 2 clearly suggest that the extent of the unstable range of parameters continuously increases as the Reynolds number is raised, and that in the limit of vanishing viscosity ($Re \to \infty$), it occupies the whole region located below the curve of equation $k = -m/q$. This behaviour has also been observed for $m = -3$ and -4, and it is expected to occur for all negative azimuthal wavenumbers.

To extend the description of the unstable region to larger Reynolds numbers, it can be noted that both the most unstable modes (with fixed Re, q) and the mode corresponding to marginal stability (with fixed Re and critical swirl number q_{crit}) lie close to the curve of equation $k = -m/2q$. This can be verified for $Re = 10^4$ (see figures 1*c*, 2*c* and table 4), and was also observed to hold for larger Reynolds numbers. Using this property, we have been able to map the unstable region in the (Re, q)-plane, for azimuthal wavenumbers $m = -1$, -2 and -3, up to $Re = 10^5$. These results, which required as much as $N = 280$ collocation points to achieve the convergence, are represented in figure 3. The curves indicate the critical swirl number q_{crit} for stabilization with fixed Reynolds number. Alternatively, they can be interpreted as an indication of the critical Reynolds number Re_{crit} for destabilization with fixed swirl number. When the Reynolds number is increased, the helical modes ($m = -1$) are the first to be destabilized. The modes with larger $|m|$ then follow.

Although the curves in figure 3 cannot be continued towards larger Reynolds numbers with the present numerical method, these results strongly suggest that as the Reynolds number goes to infinity the critical swirl number does not reach a finite

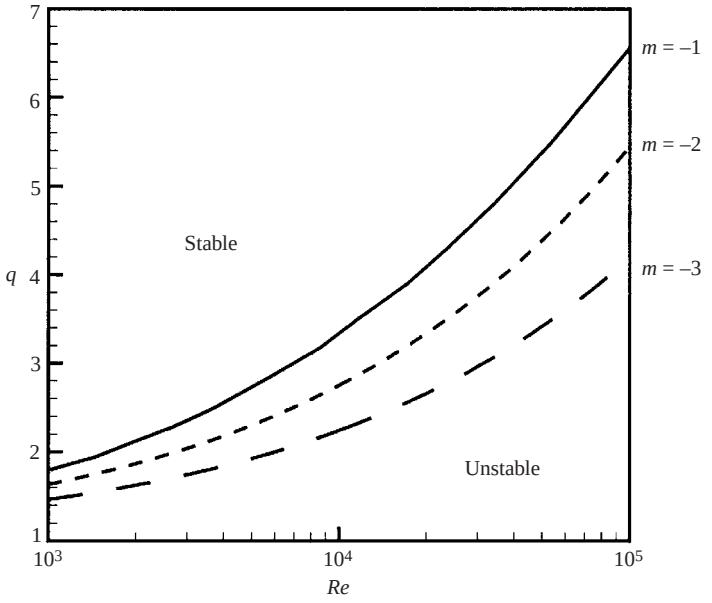

FIGURE 3. Marginal stability curves in the (Re, q)-plane for $m = -1$, -2 and -3.

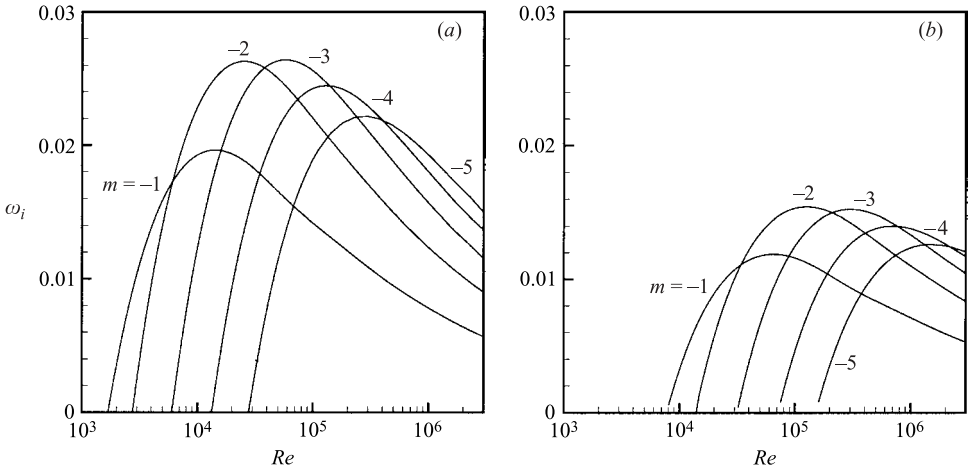

FIGURE 4. Amplification rate ω_i of the most unstable mode as function of Re for (a) $q = 2$ and (b) $q = 3$ with azimuthal wavenumbers m ranging from -1 to -5.

limit, but is continuously increasing. This is surprising because as $q \to \infty$ the q-vortex reduces to a pure vortex with no axial velocity, which is known to be inviscidly stable (Sipp 1999). However, this behaviour is confirmed by ongoing asymptotic analyses. In particular, we have been able to demonstrate that as $Re \to \infty$ the critical swirl number scales as $q_{crit} = O(Re^{1/3})$ (Fabre & Le Dizès 2004).

To end this section, we illustrate in figure 4 the variation of the amplification rate of the most unstable modes with the Reynolds numbers, with m ranging from -1 to -5. For $q = 2$ (figure 4a), the helical ($m = -1$) mode is the first to be destabilized (for $Re \approx 1500$). This mode reaches its maximum amplification $\omega_i \approx 0.01963$ for a Reynolds

number $Re \approx 1.4 \times 10^4$. The modes with $m = -2$ and $m = -3$ become unstable at larger values of the Reynolds number, but they reach higher amplification rates. The maximum values on these branches are $\omega_i = 0.02630$ and 0.02642, and they are obtained for 2.6×10^4 and 5.7×10^4, respectively. For larger $|m|$ the maximum values attained by the branches are observed to decrease. For $m = -4$ and -5, the maxima occur for 1.34×10^5 and 2.78×10^5, and correspond respectively to $\omega_i = 0.02446$ and 0.02215.

As shown in figure 4(*b*), similar trends are observed for $q = 3$. Here instabilities occur for larger Reynolds numbers and reach lower maximum amplifications. For $m = -1, -2, -3, -4$ and -5 the maximum values are $\omega_i = 0.01188$, 0.01544, 0.01525, 0.01401 and 0.01262, and the corresponding Reynolds numbers are 6.5×10^4, 1.26×10^5, 3.01×10^5, 7.14×10^5, and 1.42×10^6, respectively.

It is worth pointing out that in all cases displayed, the amplification rates of the viscous modes are but one order of magnitude smaller than those of the inviscid modes existing for $q < 1.5$ (compare with the inviscid results displayed in table 1). On the other hand, these instabilities are much more amplified than the viscous modes of Khorrami (1991), whose amplification rates are at most of order 10^{-4} in the range of Reynolds numbers considered here.

4. Nature of the instabilities

The results of the previous section are in apparent contradiction with the results of Stewartson (1982) who demonstrated that viscosity has a purely stabilizing effect on the instabilities occurring for $q < 1.5$. This paradox may be cleared up if one considers that the instabilities demonstrated here for $q > 1.5$ are of a different nature than those considered by Stewartson (1982). In this section we show some evidence that these instabilities belong to a family of viscous centre-modes which is distinct from the inviscid instabilities mapped by MP, as well as from the near-neutral inviscid modes of Stewartson & Brown (1985) and also from the viscous modes of Khorrami (1991). On the other hand, they are related to the family of viscous instabilities discovered in the swirling Poiseuille flow by SNB. To demonstrate this, we investigate the temporal instability branches and comment their similarities with the results of SNB. We then describe the structure of the modes and show that they display a centre-mode behaviour. Finally, based on these results we discuss more precisely the similarities and differences with the modes of SNB.

4.1. *Temporal branches*

In the previous section the analysis was restricted to the most amplified modes. However, as often observed for vortex instabilities, our computations also revealed the existence of secondary branches of unstable modes. Generally, they are characterized by weaker amplification rates than the primary modes and their number is an increasing function of the Reynolds number. We illustrate this point in figures 5 and 6 for various sets of parameters q, Re and m.

Figure 5(*a–c*) displays the unstable temporal branches as functions of the axial wavenumber k, for $m = -1$ and $q = 2$, and for Reynolds numbers of 10^4, 10^5 and 5×10^5. For $Re = 10^4$ there is a single unstable branch. For $Re = 10^5$ three branches are observed. For $Re = 5 \times 10^5$, there are five unstable branches, and the behaviour of the third and fourth ones is quite interesting. The third one becomes unstable at a lower neutral point $k \approx 0.06$; it reaches a maximum for $k \approx 0.08$ and then it abruptly decreases and crosses the fourth one for $k \approx 0.11$. For larger k, this branch

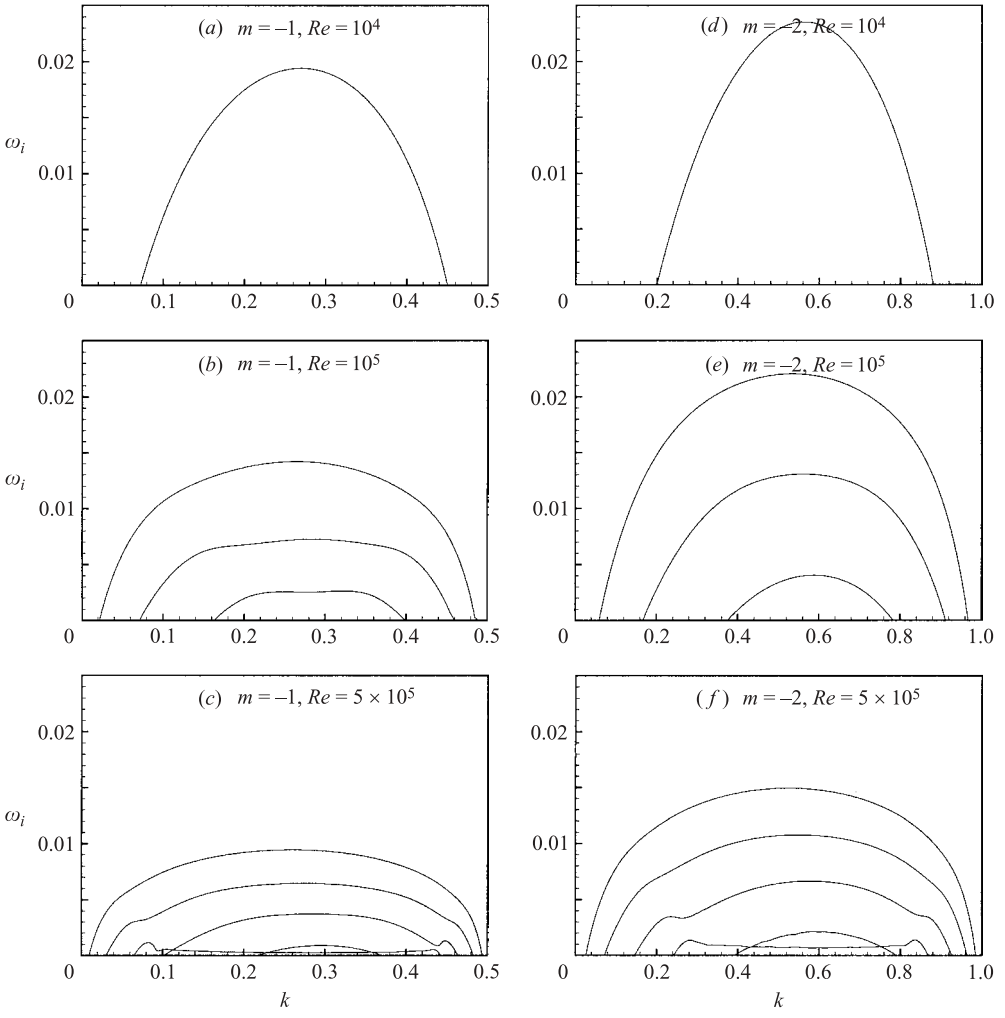

FIGURE 5. Amplification rates of unstable modes as function of wavenumber for $q = 2$ and various sets of m and Re.

remains very weakly amplified up to its upper neutral point, for $k \approx 0.44$. Near the upper neutral point, the behaviour of the third and fourth branches is similar to that observed near the lower neutral point, except that the branches avoid each other instead of crossing. These unusual features were carefully checked, and a numerical origin could be discarded. Note that a similar behaviour was observed by SNB for the swirling Poiseuille flow, and by Khorrami (1992) for the q-vortex with $q = 0.4$.

Figure 5(d–f) displays the case $m = -2$, $q = 2$. The results look similar to those for $m = -1$. For $Re = 5 \times 10^5$ one also observes a crossing, but here it occurs between the fourth and fifth branches. It is interesting to note that in all cases displayed, the unstable modes with $m = -2$ reach higher amplification rates than those with $m = -1$. This is consistent with the results displayed in figure 4 for the primary branch.

Figure 6(a–c) corresponds to the case with $m = -1$ and $q = 3$, and Reynolds numbers of 10^4, 10^5 and 10^6. Results are very similar to those displayed in figure 5(a–c) for $q = 2$. For $Re = 10^4$, only one weakly amplified mode is observed (according to figure 3 this case is close to the stability threshold). For $Re = 10^5$, two branches are

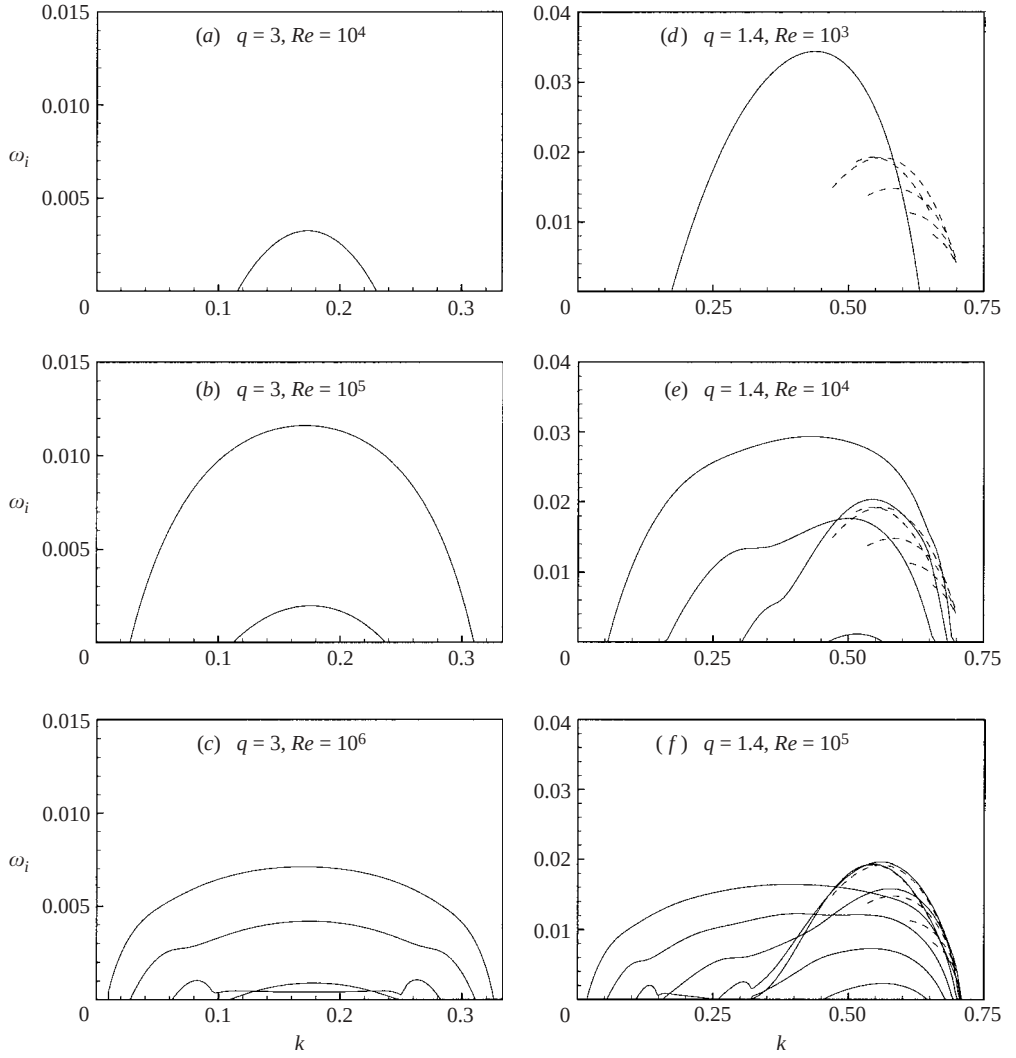

FIGURE 6. Amplification rates of unstable modes as function of wavenumber for $m = -1$ and various sets of q and Re. For $q = 1.4$ the dashed line corresponds to the inviscid results.

observed and for $Re = 10^6$ there are four. In the latter plot, we observe, again, the characteristic crossing between the third and fourth branches.

Figure 6(d–f) corresponds to $m = -1$, $q = 1.4$. This case is unstable in the inviscid limit, and inviscid results are displayed with dashed lines. Five inviscid branches were found, but due to difficulties often reported in the literature and discussed in the introduction, they could not be followed down to their neutral points (note that two of these branches display almost the same maximum value). For $Re = 10^3$, a single unstable branch is obtained. Surprisingly, this branch does not correspond to any of the inviscid modes: it occurs in a different range of wavenumbers, and its maximum of amplification is about twice that of the inviscid ones. This branch most likely belongs to the same family of viscous modes as those observed for $q > 1.5$. For $Re = 10^4$ we note the existence of four unstable modes. The most amplified one is, again, a viscous mode. On the other hand, the second mode is an inviscid one. It reaches its maximum

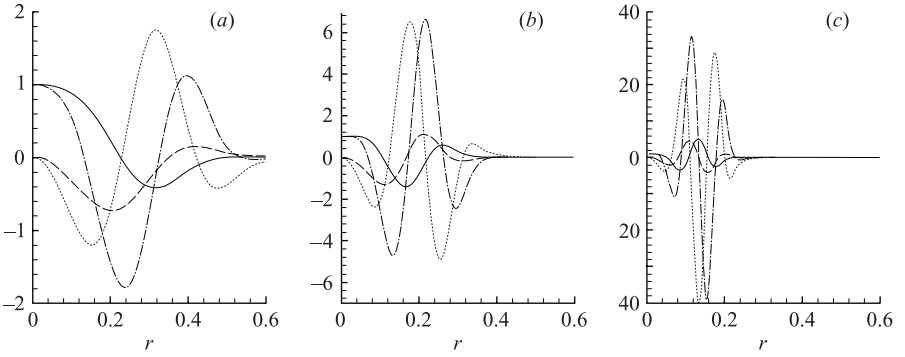

FIGURE 7. Structure of some viscous modes with $q=2$, $m=-1$, $k=0.25$. Eigenfunction components: $Re(-iu)$ (solid line), $\mathrm{Im}(-iu)$ (dashed line), $Re(v)$ (dash-dotted line), $\mathrm{Im}(v)$ (dotted line). (*a*) $Re=10^4$, $\omega_i=0.01927$; (*b*) $Re=10^5$, $\omega_i=0.01417$; (*c*) $Re=10^6$, $\omega_i=0.00780$.

amplification close to $k\approx 0.55$, $\omega_i\approx 0.02$, in agreement with the inviscid results. The third branch of instability is observed to cross the second one. This mode seems to be of a hybrid nature, as it displays partly the characteristics of the viscous modes, and partly those of the inviscid ones. A fourth weakly unstable mode also exists for $k\approx 0.5$. For $Re=10^5$ we also observe the coexistence of both viscous and inviscid modes, as well as several modes with a hybrid nature. The most amplified mode is now an inviscid one. Note, again, the characteristic crossing between the third and fourth branches of unstable modes occurring in the vicinity of the lower neutral point.

4.2. *Structure of the eigenmodes*

Figure 7 shows the eigencomponents u and v of the most amplified mode for $m=-1$, $q=2$, for Reynolds numbers ranging from 10^4 to 10^6. Two features are particularly interesting. First, as Re is raised, the structure of the mode becomes increasingly concentrated in the vicinity of the vortex centreline. For example, for $Re=10^6$, the whole structure of the mode is located within $|r|<0.25$. This fully justifies the identification of these modes as centre-modes. Secondly, the eigenvalue components become violently oscillatory and the number of oscillations is an increasing function of the Reynolds number. This feature is commonly observed in the asymptotic study of viscous modes (Drazin & Reid 1981), and it clearly demonstrates the viscous nature of the present modes. Note that the structure described here is very close to that of the viscous modes of SNB: see, in particular, their figures 6 to 9 and compare with our figure 8.

Figure 8 shows another representation of the structure of the eigenmodes, with iso-levels of the axial vorticity component $\xi_z(r,\theta)=(1/r)[\partial(rv)/\partial r - imu]\exp(im\theta+ikz)$ (in the $z=0$ plane). The most amplified helical ($m=-1$) and double-helix ($m=-2$) modes with $Re=10^4$, $q=2$ are displayed. Under this representation, the modes are observed to take the form of a tight spiral wrapped about the vortex centreline.

The trends demonstrated here (a spiral structure with increasingly strong oscillations and a collapse toward the vortex centreline) have been observed for $m=-1$, -2 and -3 for the most amplified mode, and they also hold for most of the secondary modes. However, the mode which becomes weakly amplified and crosses the following branches in figures 5(*c*), 5(*f*) and 6(*c*) has a different structure. This mode is better described as a ring mode, and its structure is similar to that of the 'inviscid singular'

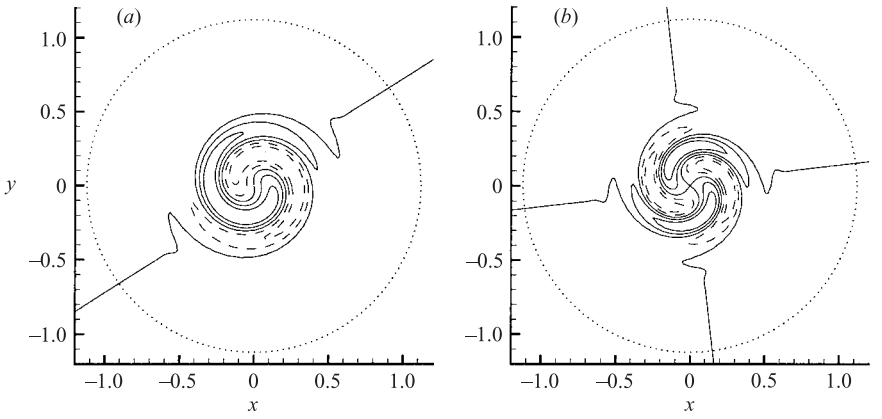

FIGURE 8. Structure of some viscous modes with $q = 2, Re = 10^4$: contours of constant axial vorticity component. Levels correspond to 0, $\pm 1/3$, and $\pm 2/3$ of the maximum value (with negative levels dashed). The dotted circles display the location of maximum azimuthal velocity in the vortex ($r_{max} = 1.1209$). (*a*) $m = -1, k = 0.25, \omega_i = 0.01927$; (*b*) $m = -2, k = 0.5, \omega_i = 0.02290$.

mode computed by SNB and displayed in their figure 5. A full description of this particular branch is left for future work.

4.3. *Discussion*

The results presented above, in particular the increasing oscillations of the eigenmode components and the irregular behaviour of the secondary modes near their upper and lower neutral points, strongly suggest that the present modes are related to the viscous modes discovered in the swirling Poiseuille flow by SNB. In the concluding sections of their paper, SNB suggested that modes related to those they had found could exist in the q-vortex, and could affect all values of the swirl number. Our results seem to confirm their expectation. However, other families of instabilities could have been invoked to explain our results, and have to be ruled out.

First, a relation with Khorrami (1991)'s viscous modes is easily discarded. These modes occur only for $m = 0$ and $m = 1$, and in a different range of swirl number. Moreover, the asymptotic study of Duck & Khorrami (1992) showed that instead of collapsing towards the centreline as $Re \to \infty$, the structure of these modes tends to a regular limit (except in the vicinity of a critical layer for $m = 1$). Finally, the amplification rates of these modes is $O(Re^{-1})$ at leading order, and such a power law is not observed for the viscous centre modes.

Let us consider, now, the near-neutral inviscid centre-modes of Stewartson & Brown (1985). According to these authors, such modes should exist in the vicinity of the curve of equation $k \approx |m|/q$, but only in discrete intervals of the swirl number q. In each of these intervals, the amplification rate of these modes should follow a law of the form $\omega_i = O(|m|/q - k)^{p+1}$ with $p^2 = m^2 + 8q^2/(q^2 - 2)$, and according to Duck (1996) viscosity should lead to a damping of these modes for Reynolds numbers scaling as $Re = O(|m|/q - k)^{-2-p}$. For $m = -1$, the case $q = 2$ falls within one of the unstable intervals predicted by Stewartson & Brown (1985), but not the cases $q = 3$ and $q = 1.4$. Accordingly, for $q = 2$, in the limit $Re \to \infty$ some of the unstable branches should asymptote to a common limit in the vicinity of their upper neutral point. This prediction is not confirmed by our results, and similar results were obtained for $q = 2$ and for $q = 3$. In the case $q = 2$, we performed a detailed study up to $Re \approx 10^7$, but

were not able to confirm the existence of the kinds of modes predicted by Stewartson & Brown (1985). Possibly, although they are solutions of the inviscid problem with a contour deformation rule, these modes may not be reached as the limit of the viscous problem for vanishing viscosity. Such a possibility has already been hypothesized by SNB in the related problem of swirling Poiseuille flow.

Now, if the modes studied here are related to the viscous centre modes of the swirling Poiseuille flow, it may be asked whether the asymptotic results of SNB directly apply to the q-vortex. However, a detailed study shows that it is not the case, because the two flows differ in the vicinity of their centreline. For the rotating Poiseuille flow, the axial velocity is given by $W=\epsilon(1-r^2)$ (ϵ being the inverse swirl number in the notation of SNB) and the azimuthal velocity is $V=r$. For the q-vortex, a Taylor series development shows that the axial velocity is $W=1-r^2+O(r^4)$, thus the leading-order terms are proportional to those for the rotating Poiseuille flow. On the other hand, the Taylor series of the azimuthal velocity is $V=qr-qr^3/2+O(r^5)$. The difference may seem slight, but inspection shows that the $O(r^3)$ term, which is absent in the rotating Poiseuille, occurs at leading order in the asymptotic scaling.

So, the results of SNB cannot be directly applied to the q-vortex. On the other hand, an asymptotic treatment similar to that of SNB, but based on the relevant scalings, has been undertaken. Two directions have been explored. First, Le Dizès & Fabre (2004) have described analytically the structure of the modes away from the neutral curves on the basis of a WKBJ expansion. They have been able to generalize the analysis conducted in § 5 of SNB to an arbitrary mean flow. According to this work, the amplification rate of the viscous modes of the q-vortex is given, at leading order, by the following expression:

$$\omega_i=\frac{3}{2}\left[q^2k\left(k+\frac{m}{q}\right)\right]^{1/3}Re^{-1/3}. \tag{4.1}$$

The next term in the expansion, which is of order $Re^{-1/2}$, has also been derived. These expressions compare well with the present numerical results.

In a second direction, Fabre & Le Dizès (2004) have explored the vicinity of the lower ($k\approx 0$) and upper ($k\approx|m|/q$) neutral curves following the approach of §§ 3 and 4 of SNB, which consists of deriving a reduced system of equations for scaled variables and solving them numerically. The approach leads to an asymptotic description of the modes near the neutral conditions which does not reduce to that of SNB. In the lower neutral curve region, the study provides an estimate of the lower neutral point given by $k_-\approx 4.73q^{1/2}Re^{-1/2}$ for helical modes. For the upper neutral point, the asymptotic study indicates a scaling with the form $k_+\approx|m|/q-O(Re^{-1/2})$, but the dependence with respect to q is more intricate than for the lower neutral point. In both cases the asymptotic results are in excellent accordance with the numerical results presented here.

5. Application

Before concluding this paper, we briefly discuss the relevance of these findings to aircraft trailing wakes. As emphasized in § 2.1, real-life trailing vortices are quite different from the q-vortex model, so the present results cannot be extrapolated directly. However, due to the centre-mode nature of the present instabilities, it may be expected that their properties mainly depend on the flow conditions near the vortex axis, not on the exact velocity laws. This is, indeed, confirmed by ongoing asymptotic analyses. Based on these considerations, we may attempt to apply the present results

to more general vortices assuming that a Taylor series development of the q-vortex at $r = 0$ holds for these actual vortices.

Let us consider, for example, the wind tunnel experiment of Jacquin *et al.* (2001), already mentioned in § 2.1. In this experiment, the span of the model was $b_0 = 0.448\,\mathrm{m}$ and the nominal velocity of the wind tunnel was $U_0 = 50\,\mathrm{m\,s^{-1}}$. The maximum values of the azimuthal and axial velocities within the vortices were found to be respectively $25\%U_0$ and $10\%U_0$, and the 'inner' vortex core radius was estimated to be $1\%b_0$. This may be approximated by a q-vortex with $q \approx 4$, and $Re \approx 1500$. According to our results this leads to a stable configuration. In this experiment, vortices displayed significant meandering whose origin was not fully understood. We may conclude here that for this particular experiment, vortex meandering is probably not related to a viscous instability. It is most likely to be due to the excitation of Kelvin waves within the vortex core by the surrounding turbulence, as initially proposed by Jacquin *et al.* (2001). Now, if the data obtained in this experiment are extrapolated to a large transport aircraft (such as an Airbus A340 or a Boeing 747), with a typical span $b_0 = 60\,\mathrm{m}$ and a landing approach velocity $U_0 = 70\,\mathrm{m\,s^{-1}}$, the Reynolds number based on the vortex scales reaches $Re \approx 2.8 \times 10^5$. Retaining the same swirl number leads to unstable conditions. More specifically, for this set of parameters, the most amplified mode is a double-helix ($m = -2$) one, with a dimensionless amplification rate $\omega_i = 0.011$. This corresponds to a dimensional characteristic time scale $\tau = \omega_i^{-1} \approx 8\,\mathrm{s}$. Interestingly, this time scale is comparable to that of the inviscid cooperative instabilities. For example, under the same conditions, the characteristic time scale of the Crow instability is $\tau = 30\,\mathrm{s}$. The development of viscous instabilities in such trailing wakes could thus constitute an additional source of energy for vortex meandering.

The tentative application presented above must be considered with caution, because little is known about the properties of real trailing vortices in their central region. For example, in the experiment of Jacquin *et al.* (2001), the 'inner core' region was too small to be discriminated experimentally with confidence, and the value $1\%b_0$ was only indicative. The extrapolation of a wind tunnel experiment to a full-scale aircraft is also questionable. Due to these uncertainties, the significance of viscous instabilities in trailing vortices remains puzzling, and future investigations should be undertaken to clarify the problem. Finally, the significance of viscous instabilities in other kinds of vortices, such as for example tornadoes or coherent structures in turbulent flows, is also a matter of interest.

6. Conclusions

In this paper we have presented a numerical study of the temporal stability of a trailing line vortex for a range of parameters corresponding to large swirl numbers ($q > 1.5$) and large Reynolds numbers. In this range, which is usually assumed to be stable, we have observed the existence of viscous instabilities affecting negative azimuthal wavenumbers and small axial wavenumbers. We have described numerically the topography of these instabilities using a highly accurate Chebyshev collocation method. These results complement those of Mayer & Powell (1992) who considered smaller values of the Reynolds and swirl numbers. It is shown that while viscosity is purely stabilizing for small Reynolds numbers, it becomes destabilizing for $Re \gtrsim 10^3$. For example, for $Re = 10^4$, instabilities persist up to a critical value of the swirl number which is nearly twice the inviscid threshold $q_{crit} \approx 1.5$. Moreover, our results indicate that in the limit of very large Reynolds numbers the critical swirl number

tends to infinity. Consequently, for vanishing (but non-zero) viscosity, this kind of instability is likely to occur for all values of the swirl number q.

We have described numerically these instabilities up to $Re = 10^6$. Our results show that these instabilities take the form of centre-modes, i.e. they only affect a narrow region in the vicinity of the vortex centreline. Another interesting feature is the occurrence of secondary branches of unstable modes, some of them displaying an irregular mode-crossing behaviour in the vicinity of their neutral points. These features allow one to conclude that the present instabilities are related to a family of viscous modes studied in the swirling Poiseuille flow by Stewartson *et al.* (1988). On the other hand, they are distinct from the inviscid modes mapped by Mayer & Powell (1992), as well as from the viscous modes described by Khorrami (1991), and from the near-neutral inviscid centre-modes predicted by Stewartson & Brown (1985). For $q < 1.5$, they coexist with the family of inviscid modes, and some modes with an hybrid nature have been observed.

Finally, we have discussed the application of these results to aircraft trailing vortices. According to what is known from experiments about realistic vortex cores, the viscous instability could occur in trailing vortices, and develop on characteristic time scales comparable to those of the cooperative instabilities. Further investigations are needed to clarify their significance in the dynamics of trailing wakes.

It may appear surprising that, despite the considerable work on the subject, these instabilities have not been identified before. We attribute our success to the accuracy of our Chebyshev collocation method. As presented in § 2, this method takes advantage of the symmetry properties of the problem, and allows a regular distribution of the collocation points near the axis of symmetry. This enables modes with a complex structure in the vicinity of the axis to be captured, such as the centre-modes considered here. However, our numerical method reaches its limits for Reynolds numbers of order 10^6 or larger. An investigation of these centre-modes using asymptotic methods is in progress (Fabre & Le Dizès 2004; Le Dizès & Fabre 2004). This approach should provide a clearer picture of the instability properties in the range of very large Reynolds numbers.

The authors would like to thank Stéphane Le Dizès for the provision of unpublished asymptotic work, and for fruitful discussions during the revision of this paper.

Appendix. Components of the matrices in (2.4)

$$\mathscr{L}_{11} = k^2 - \partial_r \partial_r^*, \tag{A 1}$$

$$\mathscr{L}_{12} = \frac{m}{r^2}(1 - r\partial_r), \tag{A 2}$$

$$\mathscr{L}_{21} = \frac{m}{r^2}(1 + r\partial_r), \tag{A 3}$$

$$\mathscr{L}_{22} = k^2 + \frac{m^2}{r^2}, \tag{A 4}$$

$$\mathscr{M}_{11} = \Sigma(k^2 - \partial_r \partial_r^*) - \Sigma' \partial_r^* + k(W'' + W' \partial_r), \tag{A 5}$$

$$\mathscr{M}_{12} = 2k^2 \Omega - \frac{m}{r}\Sigma' + \frac{m}{r^2}\Sigma(1 - r\partial_r), \tag{A 6}$$

$$\mathscr{M}_{21} = k^2(2\Omega + r\Omega') - \frac{mk}{r}W' + \frac{m}{r^2}\Sigma(1 + r\partial_r), \tag{A 7}$$

$$\mathscr{M}_{22} = \Sigma\left(k^2 + \frac{m^2}{r^2}\right), \tag{A 8}$$

$$\mathscr{D}_{11} = -\partial_r\partial_r^*\partial_r\partial_r^* + 2k^2\partial_r\partial_r^* + \partial_r\left(\frac{m^2}{r^2}\partial_r^*\right) - k^2\left(k^2 + \frac{m^2}{r^2}\right), \tag{A 9}$$

$$\mathscr{D}_{12} = -\frac{m}{r}\partial_r^3 + \frac{2m}{r^2}\partial_r^2 + \left(\frac{mk^2}{r} + \frac{m^3 - 3m}{r^3}\right)\partial_r + 3\left(\frac{m - m^3}{r^4} - \frac{mk^2}{r^2}\right), \tag{A 10}$$

$$\mathscr{D}_{21} = \frac{m}{r}\partial_r^3 + \frac{2m}{r^2}\partial_r^2 - \left(\frac{mk^2}{r} + \frac{m^3 + m}{r^3}\right)\partial_r + \left(\frac{m - m^3}{r^4} - \frac{3mk^2}{r^2}\right), \tag{A 11}$$

$$\mathscr{D}_{22} = k^2\partial_r\partial_r^* + \partial_r^*\left(\frac{m^2}{r^2}\partial_r\right) + \frac{m^2}{r^4} - \left(k^2 + \frac{m^2}{r^2}\right)^2, \tag{A 12}$$

where

$$\partial_r^* = \partial_r + 1/r, \quad \Sigma(r) = m\Omega(r) + kW(r).$$

REFERENCES

Ash, R. L. & Khorrami, M. R. 1995 Vortex stability. In *Fluid Vortices* (ed. S. I. Green), chap. 8, pp. 317–372. Kluwer.

Batchelor, G. K. 1964 Axial flow in trailing line vortices. *J. Fluid Mech.* **20**, 645–658.

Canuto, C., Hussaini, Y. M., Quarteroni, A. & Zang, T. A. 1988 *Spectral Methods in Fluid Dynamics*. Springer.

Crouch, J. D. 1997 Instability and transient growth for two trailing-vortex pairs. *J. Fluid Mech.* **350**, 311–330.

Crow, S. 1970 Stability theory for a pair of trailing vortices. *AIAA J.* **8**, 2172–2179.

Delbende, I., Chomaz, J. & Huerre, P. 1998 Absolute/convective instabilities in the Batchelor vortex : a numerical study of the linear impulse response. *J. Fluid Mech.* **355**, 229–254.

Drazin, P. G. & Reid, W. H. 1981 *Hydrodynamic Stability*. Cambridge University Press.

Duck, P. W. 1996 The effect of viscosity on centre modes in the incompressible stability of a trailing line vortex. *Phys. Fluids* **8**, 1455–1463.

Duck, P. W. & Foster, M. R. 1980 The inviscid stability of a trailing line vortex. *Z. Angew. Math. Phys.* **31**, 524–532.

Duck, P. W. & Khorrami, M. R. 1992 A note on the effect of viscosity on the stability of a trailing line vortex. *J. Fluid Mech.* **245**, 175–189.

Fabre, D. 2002 Instabilités et instationnarités dans les tourbillons: Application aux sillages d'avions. PhD thesis, Université Paris VI.

Fabre, D., Cossu, C. & Jacquin, L. 2000 Spatio-temporal development of the long and short-wave vortex-pair instabilities. *Phys. Fluids* **12**, 1247–1250.

Fabre, D. & Jacquin, L. 2003 Short-wave cooperative instabilities in representative aircraft vortices. *Phys. Fluids* (submitted).

Fabre, D., Jacquin, L. & Loof, A. 2002 Optimal perturbations in a four-vortex aircraft wake in counter-rotating configuration. *J. Fluid Mech.* **451**, 319–328.

Fabre, D. & Le Dizès, S. 2004 Viscous centre modes in vortices: Asymptotic study of the vicinity of the neutral curves. In preparation.

Howard, L. N. & Gupta, A. S. 1962 On the hydrodynamic and hydromagnetic stability of swirling flows. *J. Fluid Mech.* **14**, 463–476.

Jacquin, L., Fabre, D., Geffroy, P. & Coustols, E. 2001 The properties of a transport aircraft wake in the extended nearfield: an experimental study. *AIAA Paper* 2001-1038.

Jacquin, L., Fabre, D., Sipp, D., Theofilis, V. & Vollmers, H. 2003 Instability and unsteadiness of wake vortices. *Aero. Sci. Tech.* **7**, 577–593.

Jacquin, L. & Pantano, C. 2002 Turbulence in trailing vortices. *J. Fluid Mech.* **471**.

Khorrami, M. R. 1991 On the viscous modes of instability of a trailing line vortex. *J. Fluid Mech.* **225**, 197–212.

Khorrami, M. R. 1992 Behavior of asymmetric unstable modes of a trailing line vortex near the upper neutral curve. *Phys. Fluids* A **5**, 1310–1313.

Khorrami, M. R., Malik, M. R. & Ash, R. L. 1989 Application of spectral collocation techniques to the stability of swirling flows. *J. Comput. Phys.* **81**, 206–229.

Le Dizès, S. & Fabre, D. 2004 Asymptotic analysis of viscous centre modes in vortices. In preparation.

Le Dizès, S. & Laporte, F. 2002 Theoretical predictions for the elliptic instability in a two-vortex flow. *J. Fluid Mech.* **471**, 169–201.

Leibovich, S. & Stewartson, K. 1983 A sufficient condition for the instability of columnar vortices. *J. Fluid Mech.* **126**, 335–356.

Lessen, M. & Paillet, F. 1974 The stability of a trailing line vortex. Part 2. Viscous theory. *J. Fluid Mech.* **65**, 769–79.

Lessen, M., Singh, P. & Paillet, F. 1974 The stability of a trailing line vortex. Part 1. Inviscid theory. *J. Fluid Mech.* **63**, 753–63.

Mayer, E. W. & Powell, K. G. 1992 Viscous and inviscid instabilities of a trailing vortex. *J. Fluid Mech.* **245**, 91–114 (referred to herein as MP).

Moore, D. & Saffman, P. 1973 Axial flow in laminar trailing vortices. *Proc. R. Soc. Lond.* A **333**, 491–508.

Moore, D. W. & Saffman, P. G. 1975 The instability of a straight vortex filament in a strain field. *Proc. R. Soc. Lond.* A **346**, 413–425.

Olendraru, C. & Sellier, A. 2002 Absolute–convective instabilities of the Batchelor vortex in the viscous case. *J. Fluid Mech.* **459**, 371–396.

Olendraru, C., Sellier, A., Rossi, M. & Huerre, P. 1999 Inviscid instability of the Batchelor vortex: absolute-convective transitions and spatial branches. *Phys. Fluids* **11**, 1805–1820.

Sipp, D. 1999 Instabilités dans les écoulements tourbillonnaires. PhD thesis, École polytechnique, Palaiseau, France.

Spalart, P. 1998 Airplane trailing vortices. *Annu. Rev. Fluid Mech.* **30**, 107–138.

Stewartson, K. 1982 The stability of swirling flows at large Reynolds numbers when subjected to perturbations with large azimuthal wavenumbers. *Phys. Fluids* **25**, 1953–1957.

Stewartson, K. & Brown, S. 1985 Near-neutral centre-modes as inviscid perturbations to a trailing line vortex. *J. Fluid Mech.* **156**, 387–399.

Stewartson, K. & Capell, K. 1985 On the stability of ring modes in a trailing line vortex: The lower neutral points. *J. Fluid Mech.* **156**, 369–386.

Stewartson, K. & Leibovich, S. 1987 On the stability of a columnar vortex to disturbances with large azimuthal wavenumbers: The upper neutral points. *J. Fluid Mech.* **178**, 549–566.

Stewartson, K., Ng, T. W. & Brown, S. 1988 Viscous centre modes in the stability of swirling Poiseuille flow. *Phil. Trans. R. Soc. Lond.* A **324**, 473–512 (referred to herein as SNB).

Tsai, C.-Y. & Widnall, S. E. 1976 The stability of short waves on a straight vortex filament in a weak externally imposed strain field. *J. Fluid Mech.* **73**, 721–733.

Uberoi, M. S. 1979 Mechanisms of decay of laminar and turbulent vortices. *J. Fluid Mech.* **90**, 241–255.